Chemical Physics Letters 591 (2014) 52–57

Contents lists available at ScienceDirect

Chemical Physics Letters

journal homepage: www.elsevier.com/locate/cplett

Solvent effect on the photo-induced proton transfer in 2-(N-methyl-α-iminoethyl)-phenol

Stepas Toliautas [a,*], Mindaugas Macernis [a], Juozas Sulskus [a], Leonas Valkunas [a,b]

[a] Department of Theoretical Physics, Faculty of Physics, Vilnius University, Saulėtekio 9-III, LT-10222 Vilnius, Lithuania
[b] Institute of Physics, Center for Physical Sciences and Technology, Savanorių 231, LT-02300 Vilnius, Lithuania

ARTICLE INFO

Article history:
Received 7 September 2013
In final form 31 October 2013
Available online 11 November 2013

ABSTRACT

Effects caused by water environment on the photo-induced proton transfer in 2-(N-methyl-α-iminoethyl)-phenol molecule are investigated by means of quantum chemical calculations. After the electronic excitation, the protonated Schiff base is twisted out from the molecular plane and later reverts to the initial state. Two possible energy relaxation pathways are revealed: photon emission from the excited-state minimum, and the non-radiative conversion through the conical intersection. Accounting for the local solvent interactions introduces substantial changes of the ground- and excited-state potential energy surfaces. These changes offer an explanation for the observed formation of the intermediate photoproducts of aromatic anils in polar solvents.

1. Introduction

Photo-induced intra- and intermolecular proton transfer corresponds to chemical reactions playing an important role in molecular systems of natural and artificial origin. For instance, the intermolecular proton transfer is utilized in transformation of light energy into chemical energy in membrane proteins as a proton concentration gradient [1–3], while the intramolecular proton transfer is usually associated with photo-induced molecular twisting [4–6]. These processes are affected by the presence of external molecules in the surrounding environment to a varying degree of extent, ranging from the proton transfer via an external H-bond network [7] to a mere structural stabilization of a certain tautomeric form [8]. Notable example of a biological system employing such type of processes is the active center of bacteriorhodopsin, which is arranged in a way to be capable of performing the photo-induced proton transfer driven by light absorption of the retinal chromophore, linked to the Lys-216 site via the protonated Schiff base [9,10]. The active center of bacteriorhodopsin contains some bound water molecules which are likely to be involved in the proton transfer process [11,12]. Somewhat similar structural organization is inherent in green fluorescence protein [13].

Due to variety of factors which are able to contribute to the proton transfer in the active center of bacteriorhodopsin, model systems containing its main structural moieties (such as the Schiff base) are also extensively studied [14,15]. The photophysical properties of the system containing the protonated Schiff base are expected to be similar to that of the other intramolecularly hydrogen-bonded aromatic compounds, such as anthranilic acid [16] and 7-(2′-pyridyl)indole [17]. Strengthening of the internal hydrogen bond is observed after the initial excitation, subsequently followed by the out-of-plane deformation and in some cases leading to a conical intersection point of potential energy surfaces of the ground electronic state S_0 and the lowest excited state S_1 [18]. A review of intramolecularly hydrogen-bonded systems is presented in [17]. On the other hand, intermolecular hydrogen bonding of the photoactive system with the hydrogen-donating solvent is also prominently studied; main photophysical processes affected by such bonding are summarized in [19]. Upon photoexcitation, the intermolecular bonds can be strengthened [20] or weakened [21]. The change in bond strength has been shown to affect excitation energies [21], photo-induced electron transfer [22,23], internal conversion [24] and other processes. Consequently, intermolecular hydrogen bonding may result in changes of the energy relaxation pathways of the system [25], leading to the range of photochromic transients [26]. It is thus necessary to treat solvent locally, rather than just including the average-field effect.

Studies of the solvent-assisted proton transfer reactions have been carried out for various model systems [27,28], including 2-(N-methyl-α-iminoethyl)-phenol (MIEP) molecule in the water surroundings [29]. It has been demonstrated that the proton positioning in the O–H–N fragment of the MIEP compound in the ground electronic state (Figure 1) is sensitive to the amount of the adjacent solvent molecules. Furthermore, polar solvent can also make a direct impact on the relaxation processes of similar molecules, as demonstrated theoretically and experimentally for

* Corresponding author. Fax: +370 5 2366003.
E-mail address: stepas.toliautas@ff.vu.lt (S. Toliautas).

0009-2614/$ - see front matter © 2013 Elsevier B.V. All rights reserved.
http://dx.doi.org/10.1016/j.cplett.2013.10.084

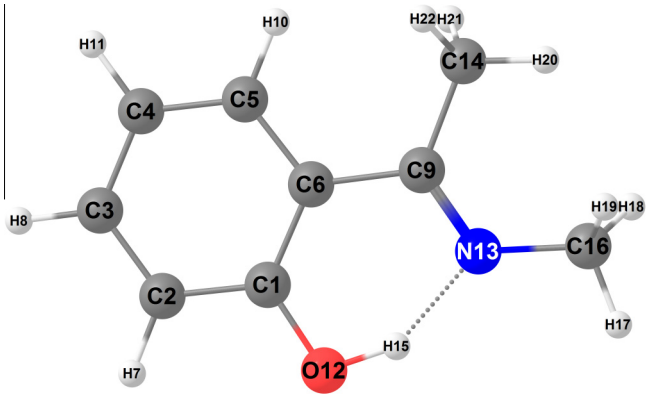

Figure 1. Molecular structure and numbering of atoms in MIEP.

N-(triphenylmethyl)-salicylidenimine in ethanol [30]. This makes MIEP suitable for the investigation of both intramolecular and intermolecular hydrogen bonding.

In this Letter we further consider the photophysical properties of the MIEP compound in water environment by analyzing the ground- and excited-state potential energy surfaces (PES) of the system. Solvent effects are treated using a continuum-based model as well as locally (by analyzing the cluster of MIEP and adjacent water molecules) and the findings are compared to each other and to the results obtained from studies of similar systems.

2. Computational details

Molecular structure optimizations of the ground-state conformations of the MIEP compound and subsequent calculations of the electronic excited states were performed by electronic structure modeling package GAUSSIAN09 [31] using density-functional theory (DFT) approach [32–34] with hybrid B3LYP functional [35]. Due to the presence of intramolecularly-bonded hydrogen, the validity of the closed-shell wavefunction was tested in the PES region of the intramolecular proton transfer. The wavefunction generated by closed-shell DFT was found to be stable (see Supplement Material for details), and the restricted method was therefore used in all calculations. Optimizations of the molecular structure in the lowest excited state were carried out using *ab initio* quantum chemistry package GAMESS [36,37] in the framework of the time-dependent DFT [38–40] with Becke's one-parameter (BOP) functional [41] and long-range electron correlation corrections (LC) [42]. Nuclear gradients used for excited-state optimization are described in [43]. Search for conical intersection points was performed using branching plane updating method, as implemented in GAMESS [44]; the main advantage of this method to the molecular energy surface calculations is that it does not require non-adiabatic coupling matrix elements. To get more reliable values for the excited-state PES, correlation consistent triple-zeta (cc-pVTZ) basis set [45] was used for calculations of vertical excitation energies of the singlet electronic states for all structures under consideration (including intermediate points along the reaction pathways). The 12 lowest states were calculated, 8 of which were used for the analysis.

Above-mentioned calculations do not take the possible environmental effects into account. Results of those calculations are hereafter referred to as the results in vacuum. To study the influence of the polar solvent field, certain computations were repeated using conductor-like polarizable continuum model (C-PCM), as implemented in GAUSSIAN09 [46], with solvent parameters of water. Additionally, local effects of the first shell of the solvent were modeled by assuming water molecules to be in the vicinity of the MIEP compound and performing a geometry optimization of the resulting cluster. It has been shown previously that the cluster of the MIEP together with 3 water molecules positioned in the vicinity of the O–H–N fragment of the compound (Figure 1) is the minimal system needed for correct description of qualitative properties of the compound in the ground electronic state [29]. In order to determine the smallest number and positions of polar solvent molecules that have the largest effect on the MIEP compound during photoexcitation, preliminary modeling by means of the ONIOM approach implemented in GAUSSIAN09 [47] was performed. Initial calculation was carried out using the two-layer model with the MIEP compound in the inner shell (described by DFT B3LYP with 6-311G(d,p) basis set) and 32 water molecules in the outer shell (described by semi-empirical PM3 theory). It was determined that the first solvent shell around the MIEP is formed by 22 water molecules. These molecules were selected for the second two-layer ONIOM calculation, employing DFT B3LYP/cc-pVTZ and Hartree–Fock/6-31G(d,p) computational levels for the inner and outer shells of the system, respectively. A twisting of the Schiff base after the excitation was simulated by optimizing geometric parameters of the system for the 9 different values of the fixed dihedral angle $d(C_1–C_6–C_9–N_{13})$ until the convergence to the order of thermal fluctuations ($\leqslant k_BT$) was achieved. Finally, the MIEP compound with 4 water molecules closely bonded to the O–H–N fragment was treated as a supermolecule and its properties were calculated at the DFT B3LYP/cc-pVTZ computational level. For correct assessment of weak molecular interactions in solvent, basis set superposition effect was investigated for both intramolecular interactions (between structural groups of MIEP) and intermolecular interactions (between MIEP and surrounding water molecules), using counterpoise method to calculate BSSE-corrected energies of the various ground-state conformations. (Full details are available in Supplement Material.)

3. Results and discussion

3.1. Molecular structure of MIEP

Molecular structure of the MIEP compound in the electronic ground state S_0 is shown in Figure 1. The main constituents of the compound are the phenol group and the Schiff base, which are situated in a common plane and are connected by a single $C_6–C_9$ bond. The potential energy function of the ground state contains two adjacent minima related to the position of H_{15} atom (proton) between O_{12} atom of the phenol group and N_{13} atom of the Schiff base. These two minima correspond to the closed enol (H_{15} bonded to O_{12}, see Figure 1) and *cis*-keto (H_{15} bonded to N_{13}) tautomeric forms of the MIEP compound. The third tautomeric form, *trans*-keto, is usually suggested as a photoproduct of the electronically excited MIEP molecule. It contains a reversed Schiff base (dihedral angle $d(C_1–C_6–C_9–N_{13}) \approx 180°$). Calculated bond lengths for the resulting structures are: $r(O_{12}–H_{15}) = 1.01$ Å, $r(N_{13}–H_{15}) = 1.64$ Å for the enol tautomer, and $r(O_{12}–H_{15}) = 1.55$ Å, $r(N_{13}–H_{15}) = 1.06$ Å for the *cis*-keto tautomer. The ratio of the O–H and N–H bond lengths in respective tautomers is typical [48] and indicates full O–H···N → O···H–N transition between the two forms. Differences of other geometric parameters are negligible.

Electronic ground-state energy values of the two forms of the MIEP compound, calculated with respect to the total energy of the *cis*-keto structure obtained using C-PCM solvent model, are as follows: enol – 0.28 eV in vacuum and 0.05 eV in water (C-PCM), *cis*-keto – 0.41 eV in vacuum. Both vacuum- and solvent-based calculations confirm the presence of a small (few k_BT) energy barrier between the two minima. The values for the barrier are: 0.17 eV (from the O_{12} side) and 0.04 eV (from the N_{13}

side) in vacuum, 0.07 and 0.11 eV in solvent (C-PCM). Accounting for the solvent also lowers the total energy of the compound and rearranges the energetic order of the adjacent structures, making the *cis*-keto tautomer slightly more favorable than the enol form in the ground state. It has been already shown in earlier study that by taking into account zero point energies during calculations, the energetic barrier between enol and *cis*-keto tautomers in the polar solvent practically disappears, while the *cis*-keto form becomes even more favorable [29].

3.2. Vertical electronic excitations

Calculated properties of vertical electronic excitations from the ground-state structures of the MIEP molecule are summarized in Figure 2 and Table 1. It is obvious from Figure 2 that the use of continuum-based solvent model results only in marginal changes to the energies and the intensities of the electronic transitions. However, as mentioned in the previous section, the solvent model favors the *cis*-keto structure of the compound in the electronic ground state S_0. Thus the comparison of the ground-state absorption spectra of the MIEP in vacuum and in the solvent reveals a strong red shift of the lowest absorption peak. The transition energy of the optically-allowed excited states S_1 and S_3 decreases from 3.98 eV (enol, vacuum) to 3.31 eV (*cis*-keto, solvent) and from 5.00 to 4.69 eV, respectively (Table 1). Furthermore, enol-to-keto decrease in the total potential energy of the S_1 state is observed both in vacuum and in the solvent. Thus, if the molecule assumes

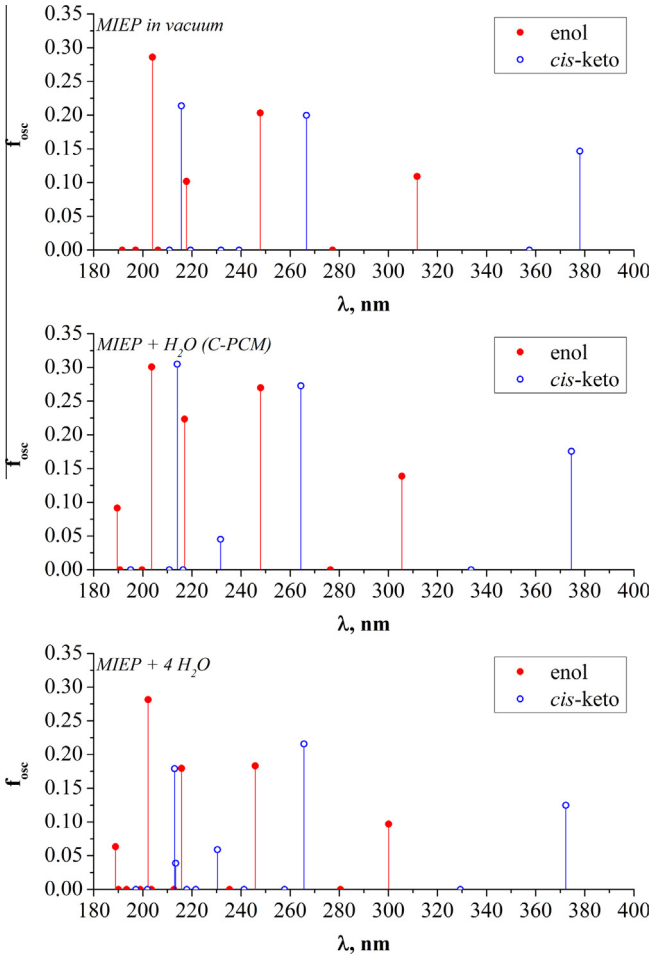

Figure 2. Electronic excited states of the MIEP compound in vacuum (top), in water (C-PCM solvent model) (middle) and as the MIEP-water cluster (bottom). Filled and open circles represent enol and *cis*-keto tautomers, respectively.

Table 1
Electronic excitations of the MIEP molecule in the ground state S_0. In the 'Transition' column, numbers 1, 2, 3... denote occupied MOs, starting from HOMO. Numbers 1′, 2′, 3′... denote unoccupied MOs, starting from LUMO.

Structure	Enol (vacuum)			*Cis*-keto (vacuum)		
State No.	E_{tr}, eV	f_{osc}	Transition	E_{tr}, eV	f_{osc}	Transition
1	3.975	0.109	1–1′ (π-π^*)	3.278	0.147	1–1′ (π-π^*)
2	4.469	0	3–1′ (n–π^*)	3.467	0	2–1′ (n-π^*)
3	4.999	0.204	2–1′ (π_N-π^*)	4.647	0.200	3–1′ (π_N-π^*)
4	5.691	0.102	1–2′ (π-π_O^*)	5.180	0	1–2′
5	6.011	0	1–3′	5.344	0	1–3′ (π-π_O^*)
	Enol (water, C-PCM)			*Cis*-keto (water, C-PCM)		
1	4.056	0.139	1–1′ (π-π^*)	3.308	0.176	1–1′ (π-π^*)
2	4.483	0	3–1′ (n-π^*)	3.713	0	2–1′ (n-π^*)
3	4.997	0.270	2–1′ (π_N-π^*)	4.687	0.273	3–1′ (π_N-π^*)
4	5.711	0.224	1–2′ (π-π_O^*)	5.349	0.045	1–2′ (π-π_O^*)
5	6.087	0.301	1–3′	5.727	0	2–2′ (n-π_O^*)

the enol conformation in the ground state, after the initial excitation to the S_1 state the compound will rapidly revert to the *cis*-keto structure via the intramolecular hydrogen transfer in the excited state [49]. Preference of the *cis*-keto form in the ground state eliminates the need for this transition.

Similar observations can be made by examining the wavefunction character of the excitations to the lowest-lying optically-allowed states. Molecular orbitals (MOs) corresponding to such excitations in vacuum are shown in Figure 3. In all cases, excitation to the S_1 state corresponds to the transition between HOMO and LUMO (π-π^* transition), which results in charge redistribution towards the Schiff base. In the case of the *cis*-keto tautomer, the electron density of HOMO extends to the C_9 atom. This makes the π-system over the phenol group of the *cis*-keto tautomer larger and thus explains the decrease in the S_0–S_1 excitation energy. The shape of LUMO, however, is nearly indistinguishable between enol and *cis*-keto tautomers – notably, there is no charge redistribution along the O-H-N fragment. This confirms the prediction of the intramolecular hydrogen transfer (during which only the atom, but not the electronic density, is displaced) in the excited state S_1. Finally, molecular orbitals obtained using the averaged solvent

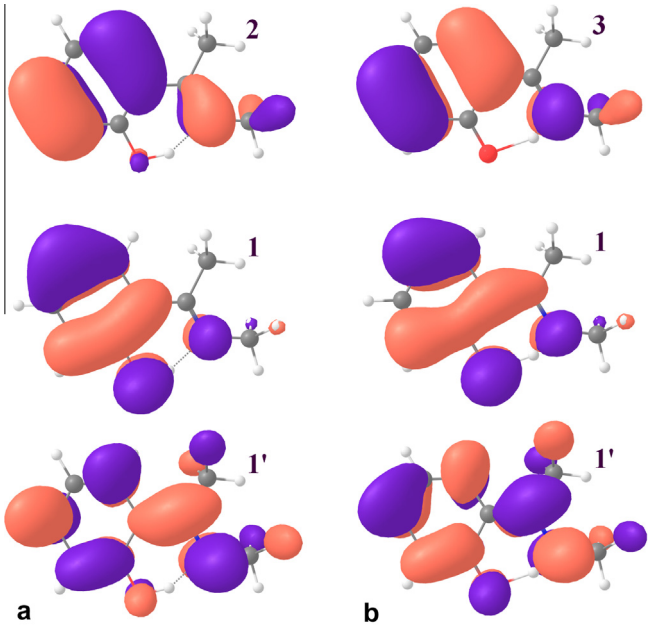

Figure 3. Selected molecular orbitals of the MIEP ground-state structures in vacuum: (a) enol, (b) *cis*-keto.

model are almost identical to the MOs generated during vacuum calculations. Therefore, the reason for the preference of the tautomeric structure is not readily apparent from calculations in vacuum and by using the C-PCM model.

3.3. Twisting of MIEP

Curvature of the potential energy surface of the first excited state S_1 in the region of the ground state energy minimum indicates the start of the structural deformation process of the MIEP molecule. The deformation involves twisting around the single C_6–C_9 bond (Figure 1), which moves the Schiff base and the phenol group out of the common plane. The deformation can thus be described qualitatively by a single reaction coordinate, corresponding to the change of a dihedral angle $d(C_1–C_6–C_9–N_{13}) \equiv d_{CCCN}$. Exploring the resulting reaction path reveals another local minimum of the ground-state energy, corresponding to the *trans*-keto structure. However, this structure is not fully planar ($d_{CCCN} = -170.8°$). Correcting for BSSE between molecular groups of the MIEP results in a small (~0.07 eV) shift of the ground-state energy. However, the shift is almost constant and thus does not influence the shapes of the resulting potential energy surfaces.

The most important features of the potential energy surfaces of the MIEP compound are gathered in Figure 4. The *cis*-keto and *trans*-keto minima of the ground state PES are separated by a transition structure (TS), located almost midway along the reaction pathway ($d_{CCCN} = -90.4°$). Points following the reaction path and connecting the three structures are marked by the filled circles in Figure 4. The S_0–S_1 excitation energy is further lowered as a result of the structural deformation and reaches the minimum value of 1.33 eV at the TS. The investigation of the region around the TS reveals additional important points of the PES. The first one corresponds to the conical intersection between the states S_0 and S_1 ($d_{CCCN} = -104.0°$). Transition from the intersection point to the global ground-state minimum (marked by open circles on the dashed line in Figure 4) is found to be barrier-less. The second significant PES point is the global minimum of the S_1 energy ($d_{CCCN} = -98.5°$). Both points are somewhat off the *cis*–*trans* reaction path, differing from the TS mostly due to the shape of the Schiff base.

Full details of the electronic excitations at the twisted structures and associated molecular orbitals are provided in Section 3 of Supplement Material. Excitation to the lowest state S_1 now corresponds to the transition between slightly modified π orbital (denoted $\pi^{\sim}$) and newly formed n_N^* orbital that is spread over the Schiff base and the C_6–C_9 bond. The transition energy value is closely related to the electronic density of the corresponding MOs around the C_6–C_9 bond – larger overlap of HOMO and LUMO in the area of the bond leads to the lower transition energy (or even to the intersection of S_0 and S_1 surfaces) and vice versa. Thus the S_0–S_1 transition can be described by the charge redistribution along the C_6–C_9 bond. The presence of the non-avoided intersection in the vicinity of the excited-state minimum and similarities of the two PES points suggest the existence of two competing energy relaxation pathways in the system.

Inclusion of the C-PCM model lessens the overlap between molecular orbitals participating in the S_0–S_1 transition at the S_1 minimum structure, which confines electronic density to the separate groups of the MIEP compound and increases the S_0–S_1 transition energy. On the potential energy surface this is observed as the decrease of the ground-state energy value compared to the vacuum calculations (from 2.33 to 1.67 eV), while the excited-state energy value remains similar (2.45 eV in vacuum, 2.52 eV using C-PCM model) (Figure 5). Overall arrangement of the PES points and of respective S_1 energies obtained using solvent model is similar to that of the vacuum calculations. Even the minimum of the state S_1 is found at almost the same place on the PES ($d_{CCCN} = -99.2°$).

3.4. Local effects of the solvent

Modeling of the MIEP compound in the water environment by using ONIOM established the structure of the first solvent shell, containing 22 molecules (Figure 6). Three water molecules are bonded to the oxygen atom of the MIEP regardless of the deformation angle d_{CCCN} (Figure 6, left). After sufficient twisting of the Schiff base out of the common plane ($d_{CCCN} > 30°$) the proton of the Schiff base is also bonded to a single additional water molecule (Figure 6, right). These 4 water molecules were selected as part of the MIEP-4H_2O cluster for further calculations. Significance of the weak molecular interactions in the hydrogen-bonded cluster was investigated by calculating BSSE-corrected ground-state energies of the cluster conformations. The corrections yielded ~0.5 eV change in energy, which again was constant for all structures under consideration. The remaining water molecules form a weakly-bound shell around the cluster (hydrogen bond lengths of 2.5–3.0 Å).

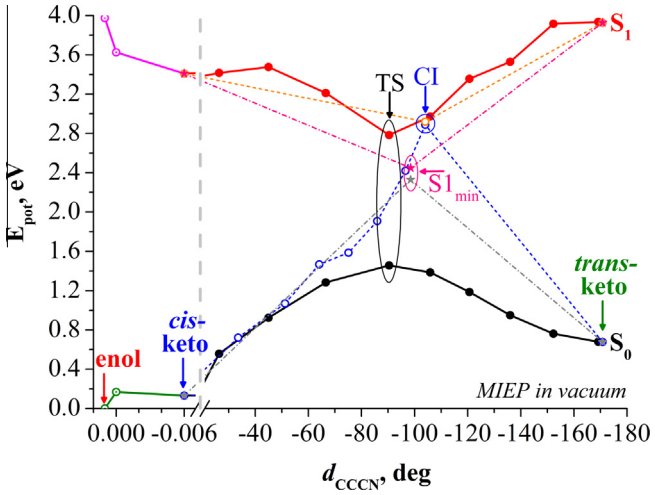

Figure 4. Potential energy surfaces of the ground (S_0) and first excited (S_1) states of the MIEP compound in vacuum. Solid and dashed lines represent different pathways on the PES. *TS* denotes transition structure between *cis*-keto and *trans*-keto tautomers, *CI* – S_0-S_1 conical intersection, $S1_{min}$ – global minimum of S_1.

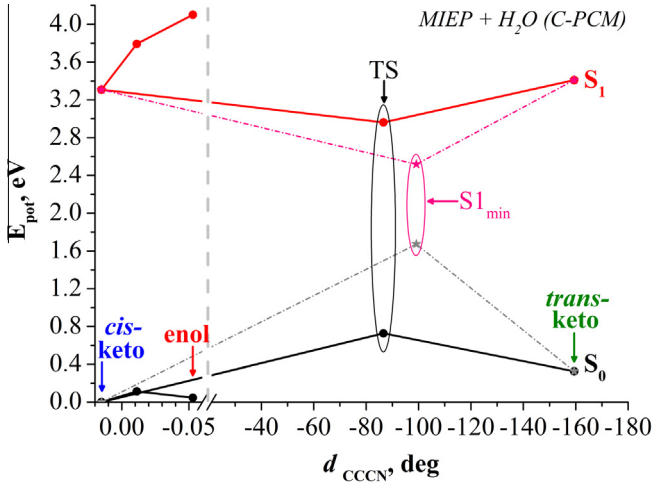

Figure 5. Potential energy surfaces of the ground (S_0) and first excited (S_1) states of the MIEP compound in water (calculated using C-PCM solvent model). Solid and dashed lines represent different pathways on the PES. *TS* denotes transition structure between *cis*-keto and *trans*-keto tautomers, $S1_{min}$ – global minimum of S_1.

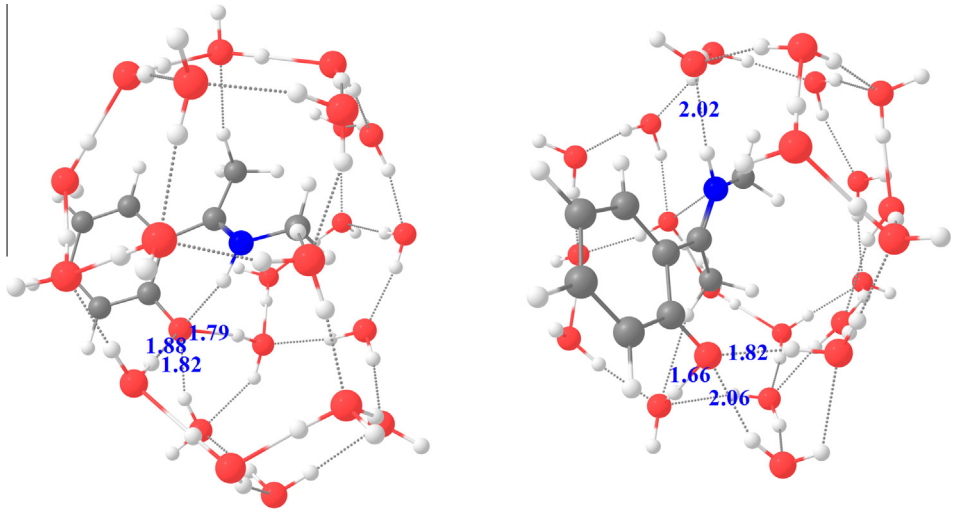

Figure 6. The network of water molecules in the vicinity of the MIEP molecule close to the *cis*-keto configuration (left) and in *trans*-keto configuration (right). The strongest hydrogen bonds are denoted in Å.

Potential energy surfaces of the MIEP-4H_2O cluster for the different values of the dihedral angle d_{CCCN} are presented in Figure 7. The surface of the ground state S_0 is strikingly different from the one obtained in vacuum. The surface is almost flat (all values are less than 0.03 eV higher than S_0 energy of *cis*-keto tautomer) yet complicated, containing 3 local minima in addition to the optimal *cis*-keto structure. Since the shape of the S_0 surface obtained using the C-PCM solvent model was similar to the vacuum case, this result demonstrates a strong local influence of the polar solvent on the MIEP: water molecules change their positions, adapting to the structure of the twisted compound. Furthermore, the *trans*-keto structure is markedly non-planar, with angle $d_{CCCN} \approx -150°$. However, a very similar molecule (without the nitrogen-bonded methyl group) is reported to have the planar *trans*-keto tautomer even when directly interacting with water [50]. In the current case, the presence of the second methyl group leads to an unstable C_s symmetry in the *trans*-keto form, which is likely to break down under the influence of the polar solvent. Meanwhile, the S_1 state surface is qualitatively similar to the results shown in Figure 4 and Figure 5.

Properties of the vertical electronic excitations for the two tautomeric forms of the MIEP-4H_2O cluster are presented in the bottom panel of Figure 2. (Full results, as well as molecular orbitals associated with the lowest excitations, can be found in Section 4 of Supplement Material.) The electronic spectrum is qualitatively similar to the results obtained in vacuum and using the C-PCM solvent model (Figure 2), but is shifted by a few nanometers to higher energies because of the interaction of the excited-state electronic density of the compound with the atoms fixed in the stationary solvent shell. However, a look at the molecular orbitals of the cluster reveals that the HOMO of the *cis*-keto tautomeric form includes oxygen atoms of the two out of three hydrogen-bonded water molecules. Compared to the shape of HOMO of the enol tautomer, which does not extend to the water molecules, this result demonstrates stronger interaction with the solvent. Moreover, hydrogen bond to one of the water molecules in the *cis*-keto tautomer (1.90 Å) is significantly shorter than in the case of the enol tautomer (2.55 Å), thus resembling excited-state intermolecular hydrogen bond strengthening mechanism [19]. These features explain the preference of the ground-state structure that was indicated – but not explained – by the results of the average-field model.

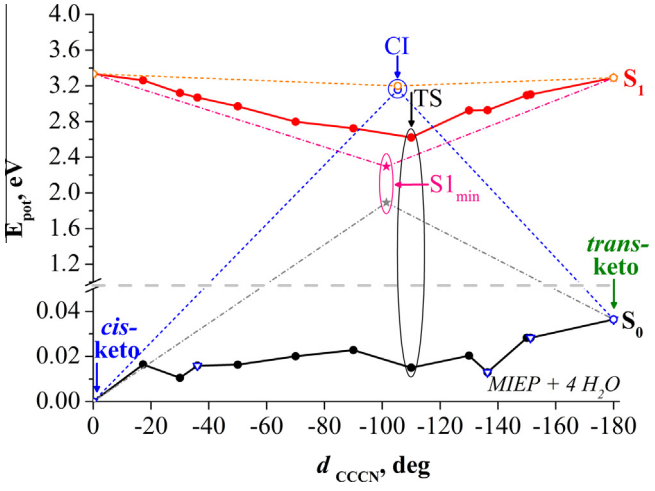

Figure 7. Potential energy surfaces of ground (S_0) and first excited (S_1) states of the MIEP-4H_2O cluster. Downward triangles mark positions of the local minima on the S_0 surface. Solid and dashed lines represent different pathways on the PES. *TS* denotes transition structure between *cis*-keto and *trans*-keto tautomers, *CI* – S_0-S_1 conical intersection, $S1_{min}$ – global minimum of S_1.

Points of the conical intersection between states S_0 and S_1 and the energy minimum of the S_1 state of the MIEP-4H_2O cluster are located at $d_{CCCN} = -105.4°$ and $d_{CCCN} = -101.4°$, respectively (Figure 7). The ground-state potential energy value of the $S1_{min}$ structure (1.89 eV) is slightly higher than the value calculated using the C-PCM solvent model. However, the potential energy of the S_1 state for this structure (2.29 eV) is somewhat lower in comparison with the vacuum or C-PCM results. This change can be attributed to the local interaction with the solvent molecules. First, HOMO and LUMO of the MIEP-4H_2O cluster more closely resemble the MOs obtained using the continuum-based solvent model than those defined from vacuum calculations (cf. Supplement Material). This, along with the similar ground-state energy value, shows that modeling the solvent environment by 4 appropriately-positioned water molecules brings out major qualitative properties of the solvent–solute interactions. Second, HOMO of the MIEP-4H_2O cluster extends to the oxygen atom of one of the water molecules similarly to the case of the *cis*-keto tautomer. Furthermore, at the S_1 energy minimum the above-mentioned water molecule forms hydrogen bond ($r = 2.07$ Å) with the O_{12} atom. On the other hand, the potential energy of the S_0-S_1 conical intersection (3.2 eV) is not lowered by the inclusion of solvent molecules, and the intersection point shifts upward of the *cis–trans* reaction path (Figure 7). Therefore, the presence of the solvent favors the formation of the transient

structure (corresponding to the excited-state minimum) to the radiationless conversion to the ground state. Finally, while the lowest energy minimum of the first excited state was found to be similar to the minimum obtained by vacuum calculations, the existence of other excited-state minima, created during the interaction with solvent molecules, should not be excluded.

The main photophysical properties of the MIEP compound are in good agreement with the experimentally observed features of the other aromatic anil – N-(triphenylmethyl)-salicylidenimine (MS1) [30]. The excitation of MS1 in ethanol leads to the formation of different short-lived transients and long-lived photoproducts with absorption peak shifted by 20–30 nm to the longer wavelengths. S_0-S_1 transition energy values at the ground-state potential energy minima shown in Figure 7 fit this data quite well: calculated S_0–S_1 energy differences from the *cis*-keto structure are 0.28 eV (34 nm) and 0.42 eV (54 nm) for the d_{CCCN} values of 36.0° and 136.4°, respectively. Photoproducts of MS1 are also shown to be different from the *trans*-keto structure. This finding is in agreement with the PES of the MIEP (Figure 7). The comparison of the results allows us to suggest that the hydrogen-bonding of several polar solvent molecules to the photochromic compound may be responsible for creation of experimentally observed photoproducts in polar solutions of aromatic anils.

4. Conclusions

Study of the MIEP compound in water environment established that the presence of solvent itself has only minute effect on the absorption spectrum of a particular structural conformation of the compound. However, in water surroundings the *cis*-keto tautomer is favored against the enol tautomer, as opposed to the vacuum case, where the lowest potential energy corresponds to the enol form. This effect is evident in the results of both used solvent models, with findings of the MIEP-water cluster providing an explanation for the structural preference.

The photoexcitation process of the MIEP involves twisting of the compound with the Schiff base moving out of the principal plane. Subsequent energy relaxation can occur either through the excited-state minimum or by non-radiative decay via the conical intersection of the ground- and first excited-state surfaces. Transition from the first excited state is of π-n^* character and involves charge redistribution along the twisted C–C bond. In the case of decay through the conical intersection wavefunctions of the initial and final states in the area of C–C bond overlap, enabling internal conversion process.

After investigating the effects of the polar solvent during the deformation of the MIEP compound it is concluded that the hydrogen-bonding of a few solvent molecules to the active sites of the compound changes the shape of the PES along the reaction pathway and is mainly responsible for the formation of long-living photoproducts in aromatic anils. It is worth mentioning that for the full analysis of photodynamical processes in biomolecules containing the Schiff base, solution environment is best treated by using dynamical methods. However, comparison with experimental data shows that the study of the potential energy surfaces is sufficient for the qualitative explanation of the processes in the molecules after photoexcitation.

Acknowledgments

The work has been partially financed by the Lithuanian–Latvian–Taiwan project TAP-LLT-12-003. The public access supercomputer from the High Performance Computing Center (HPCC) of the Lithuanian National Center of Physical and Technology Sciences (NCPTS) at Physics Faculty of Vilnius University was used.

Appendix A. Supplementary data

Supplementary data associated with this article can be found, in the online version, at http://dx.doi.org/10.1016/j.cplett.2013.10.084.

References

[1] K. Schulten, W. Humphrey, M. Logunov, M. Sheves, D. Xu, Isr. J. Chem. 35 (1995) 447.
[2] M. Wikström, Curr. Opin. Struct. Biol. 8 (1998) 480.
[3] T.E. Decoursey, Physiol. Rev. 83 (2003) 475.
[4] V. Gulbinas, G. Kodis, L. Valkunas, A. Gruodis, J.C. Mialocq, S. Pommeret, T. Gustavsson, J. Phys. Chem. 103 (1999) 3969.
[5] A.L. Sobolewski, W. Domcke, in: T. Elsaesser, H.J. Bakker (Eds.), Ultrafast Hydrogen Bonding Dynamics And Proton Transfer Processes in the Condensed Phase, Kluwer Academic Publishers, Dordrecht, 2002, p. 93.
[6] S.-H. Yin, Y. Liu, W. Zhang, M.-X. Guo, P. Song, J. Comput. Chem. 31 (2010) 2056.
[7] C. Tanner, C. Manca, S. Leutwyler, Science 302 (2003) 1736.
[8] C. Reichardt, Solvents and Solvent Effects In Organic Chemistry, Wiley, Weinheim, 2006.
[9] R. Neutze, E. Pebay-Peyroula, K. Edman, A. Royant, J. Navarro, E.M. Landau, Biochim. Biophys. Acta 1565 (2002) 144.
[10] S. Hayashi, E. Tajkhorshid, K. Schulten, Biophys. J. 85 (2003) 1440.
[11] S. Hayashi, I. Ohmine, J. Phys. Chem. B 104 (2000) 10678.
[12] K. Murata, Y. Fujii, N. Enomoto, M. Hata, T. Hoshino, M. Tsuda, Biophys. J. 79 (2000) 982.
[13] N. Agmon, Biophys. J. 88 (2005) 2452.
[14] A. Koll, Int. J. Mol. Sci. 4 (2003) 434.
[15] I. Krol-Starzomska, A. Filarowski, M. Rospenk, A. Koll, S. Melikova, J. Phys. Chem. A 108 (2004) 2131.
[16] A.L. Sobolewski, W. Domcke, J. Phys. Chem. A 108 (2004) 10917.
[17] A.L. Sobolewski, W. Domcke, J. Phys. Chem. A 111 (2007) 11725.
[18] A.L. Sobolewski, W. Domcke, C. Dedonder-Lardeux, C. Jouvet, Phys. Chem. Chem. Phys. 4 (2002) 1093.
[19] G.-J. Zhao, K.-L. Han, Acc. Chem. Res. 45 (2012) 404.
[20] G.-J. Zhao, K.-L. Han, J. Phys. Chem. A 111 (2007) 2469.
[21] G.-J. Zhao, K.-L. Han, Chem. Phys. Chem. 9 (2008) 1842.
[22] G.-J. Zhao, J.-Y. Liu, L.-C. Zhou, K.-L. Han, J. Phys. Chem. B 111 (2007) 8940.
[23] Y.-H. Liu, S.-C. Lan, Comput. Chem. 1 (2013) 1.
[24] G.-J. Zhao, K.-L. Han, J. Phys. Chem. A 111 (2007) 9218.
[25] V. Ludwig, M.S.d. Amaral, Z.M.d. Costa, A.C. Borin, S. Canuto, L. Serrano-Andres, Chem. Phys. Lett. 463 (2008) 201.
[26] M. Ziolek, J. Kubicki, A. Maciejewski, R. Naskrecki, A. Grabowska, Phys. Chem. Chem. Phys. 6 (2004) 4682.
[27] N. Markova, V. Enchev, J. Mol. Struct. Theochem. 679 (2004) 195.
[28] A. Lewanowicz, A. Olszowski, P. Dziekonski, J. Leszcynski, J. Mol. Model. 11 (2005) 398.
[29] M. Macernis, B.P. Kietis, J. Sulskus, S.H. Lin, M. Hayashi, L. Valkunas, Chem. Phys. Lett. 466 (2008) 223.
[30] R. Karpicz, V. Gulbinas, A. Lewanowicz, M. Macernis, J. Sulskus, L. Valkunas, J. Phys. Chem. A 115 (2011) 1861.
[31] M.J. Frisch et al., Gaussian 09, Revision D.01, Gaussian Inc., Wallingford CT, 2013.
[32] P. Hohenberg, W. Kohn, Phys. Rev. 136 (1964) B864.
[33] W. Kohn, L.J. Sham, Phys. Rev. 140 (1965) A1133.
[34] R.G. Parr, W. Yang, Density-Functional Theory of Atoms and Molecules, Oxford Univ. Press, Oxford, 1989.
[35] P.J. Stephens, F.J. Devlin, C.F. Chabalowski, M.J. Frisch, J. Phys. Chem. 98 (1994) 11623.
[36] M.W. Schmidt et al., J. Comp. Chem. 14 (1993) 1347.
[37] M.S. Gordon, M.W. Schmidt, in: C.E. Dykstra, G. Frenking, K.S. Kim, G.E. Scuseria (Eds.), Theory and Applications of Computational Chemistry: The First Forty Years, Elsevier, Amsterdam, 2005, p. 1167.
[38] E. Runge, E.K.U. Gross, Phys. Rev. Lett. 52 (1984) 997.
[39] M.E. Casida, C. Jamorski, K.C. Casida, D.R. Salahub, J. Chem. Phys. 108 (1998) 4439.
[40] R.E. Stratmann, G.E. Scuseria, M.J. Frisch, J. Chem. Phys. 109 (1998) 8218.
[41] A.D. Becke, Phys. Rev. A38 (1988) 3098.
[42] Y. Tawada, T. Tsuneda, S. Yanagisawa, Y. Yanai, K. Hirao, J. Chem. Phys. 120 (2004) 8425.
[43] M. Chiba, T. Tsuneda, K. Hirao, J. Chem. Phys. 124 (2006) 144106.
[44] S. Maeda, K. Ohno, K. Morokuma, J. Chem. Theory Comput. 6 (2010) 1538.
[45] T.H. Dunning Jr., J. Chem. Phys. 90 (1989) 1007.
[46] M. Cossi, N. Rega, G. Scalmani, V. Barone, J. Comp. Chem. 24 (2003) 669.
[47] S. Dapprich, I. Komaromi, K.S. Byun, K. Morokuma, M.J. Frisch, J. Mol. Struct. (Theochem.) 462 (1999) 1.
[48] J.A. Dean, Lange's Book of Chemistry, 15th ed., McGraw-Hill, Inc., New York, 1999. pp. 4.39.
[49] M.Z. Zgierski, J. Chem. Phys. 115 (2001) 8351.
[50] J. Grzegorzek, A. Filarowski, Z. Mielke, Phys. Chem. Chem. Phys. 13 (2011) 16596.